Supporting Information

Tuning Single-Molecule Conductance via Substituents at the 1-Position of a 2,5-Diarylpyrrole Core

Ya-Hui Zhang,[a] Gui-Lan He,[a] Ye-Hao Ding,[a] Wen-Rui Xu,[a] Jian-Feng Yan,*[,a] Qian-Chong Zhang,[b,c] Yuan-Ming Li,[a] and Yao-Feng Yuan*[,a]

([a] *Key Laboratory of Molecule Synthesis and Function Discovery, Fujian Province University, College of Chemistry at Fuzhou University, Fuzhou, Fujian, 350108, China*)
([b] *State Key Laboratory of Structural Chemistry, Fujian Institute of Research on the Structure of Matter, Chinese Academy of Sciences, Fuzhou, Fujian 350002, China.*)
([c] *Institute of Molecular Engineering Plus, College of Chemistry, Fuzhou University, Fuzhou, Fujian, 350108, China.*)

Email: yanjianfeng@fzu.edu.cn, Yaofeng_yuan@fzu.edu.cn.

Table of Contents

1. Synthetic procedures

The precursor 2,5-dibromo-N-(4-R-phenyl)pyrrole (R = NMe_2, OMe, H, F, CHO, COOEt) was prepared according to the literature procedure.[1, 2]

1.1 Synthesis of 4-(2,5-bis(4-(methylthio)phenyl)-1H-pyrrol-1-yl)-N,N-dimethylaniline (**BTPP-NMe_2**)

A 100 mL three-necked flask was charged with a magnetic stir bar, (4-(methylthio)phenyl)boronic acid (MTPBA, 266.1 mg, 1.58 mmol), tetrakis(triphenylphosphine)palladium(0) $Pd(PPh_3)_4$, 46.2 mg, 0.04 mmol), and K_2CO_3 (298.1 mg, 2.16 mmol). The flask was placed under a nitrogen atmosphere using standard Schlenk techniques. 4-(2,5-dibromo-1H-pyrrol-1-yl)-N,N-dimethylaniline (250.0 mg, 0.72 mmol) was dissolved in THF (40 mL) and injected into the reaction system via a syringe, followed by dropwise addition of deionized water (10 mL). The resulting mixture was sealed into a tube and stirred at 60 °C for 48 h. After cooling, the mixture was diluted with H_2O (20 mL) and extracted with DCM (3 × 30 mL). The combined organic layers were washed with equal volumes of brine and H_2O, dried over anhydrous Na_2SO_4, filtered, and concentrated. The residue was purified by flash column chromatography (silica gel, 100–200 mesh, PE/DCM = 10:1, v/v) to afford **BTPP-NMe_2** as a white solid (266.6 mg, 0.62 mmol, 86% yield). m.p. 192–193 °C. ^{1}H NMR (500 MHz, $CDCl_3$) δ 7.13–6.93 (m, 8H, phenyl-H), 6.89 (d, J = 8.9 Hz, 2H, phenyl-H), 6.65–6.48 (m, 2H, phenyl-H), 6.43 (s, 2H, pyrrole-H), 2.96 (s, 6H, -NMe_2), 2.44 (s, 6H, -SMe). ^{13}C NMR (126 MHz, $CDCl_3$) δ 149.5, 135.9, 135.6, 130.5, 129.4, 129.0, 127.9, 126.1, 112.2, 109.4, 40.6, 15.9; HRMS (ESI^+) m/z calcd for $C_{26}H_{26}N_2S_2$: 431.1610 $[M]^+$; found 431.1609.

1.2 Synthesis of 1-(4-methoxyphenyl)-2,5-bis(4-(methylthio)phenyl)-1H-pyrrole (**BTPP-OMe**)

Following the general procedure described for **BTPP-NMe_2**, reaction of 2,5-dibromo-1-(4-methoxyphenyl)-1H-pyrrole (250.0 mg, 0.80 mmol), MTPBA (295.7 mg, 1.76 mmol), $Pd(PPh_3)_4$ (46.2 mg, 0.04 mmol), and K_2CO_3 (331.2 mg, 2.40 mmol), followed by purification, afforded **BTPP-OMe** as a white solid (263.9 mg, 0.63 mmol, 79% yield). m.p. 162–163 °C. ^{1}H NMR (500 MHz, $CDCl_3$) δ 7.06 (d, J = 8.4 Hz, 4H, phenyl-H), 7.02–6.92 (m, 6H, phenyl-H), 6.78 (d, J = 8.8 Hz, 2H, phenyl-H), 6.43 (s, 2H, pyrrole-H), 3.80 (s, 3H, -OMe), 2.44 (s, 6H, -SMe). ^{13}C NMR (126 MHz, $CDCl_3$) δ

158.7, 136.3, 135.6, 131.9, 130.2, 129.9, 129.1, 126.1, 114.2, 109.6, 55.5, 15.8. HRMS (ESI^+) m/z calcd for $C_{25}H_{23}NOS_2$: 418.1294 $[M]^+$; found 418.1294.

1.3 Synthesis of 2,5-bis(4-(methylthio)phenyl)-1-phenyl-1H-pyrrole (**BTPP-H**)

Following the general procedure for **BTPP-NMe$_2$**, reaction of 2,5-dibromo-1-phenyl-1H-pyrrole (250.0 mg, 0.83 mmol), MTPBA (306.8 mg, 1.83 mmol), $Pd(PPh_3)_4$ (46.2 mg, 0.04 mmol), and K_2CO_3 (343.6 mg, 2.49 mmol) afforded **BTPP-H** as a white solid (267.0 mg, 0.69 mmol, 83% yield). m.p. 201–202 °C. ^{1}H NMR (500 MHz, $CDCl_3$) δ 7.40–7.17 (m, 2H, phenyl-H), 7.04 (t, *J* = 7.6 Hz, 6H, phenyl-H), 6.96 (d, *J* = 8.4 Hz, 4H, phenyl-H), 6.45 (s, 2H, pyrrole-H), 2.44 (s, 6H, -SMe). ^{13}C NMR (126 MHz, $CDCl_3$) δ 139.0, 136.4, 135.4, 130.1, 129.1(3C), 127.5, 126.1, 110.0, 15.8. HRMS (ESI^+) m/z calcd for $C_{24}H_{21}NS_2$: 388.1188 $[M]^+$; found 388.1187.

1.4 Synthesis of 1-(4-fluorophenyl)-2,5-bis(4-(methylthio)phenyl)-1H-pyrrole (**BTPP-F**)

Following the general procedure for **BTPP-NMe$_2$**, reaction of 2,5-dibromo-1-(4-fluorophenyl)-1H-pyrrole (250.0 mg, 0.78 mmol), MTPBA (288.3 mg, 1.72 mmol), $Pd(PPh_3)_4$ (46.2 mg, 0.04 mmol), and K_2CO_3 (322.9 mg, 2.34 mmol) afforded **BTPP-F** as a pale yellow solid (234.1 mg, 0.58 mmol, 74% yield). m.p. 174–176 °C. ^{1}H NMR (500 MHz, $CDCl_3$) δ 7.07 (d, *J* = 8.2 Hz, 4H, phenyl-H), 7.04–6.92 (m, 8H, phenyl-H), 6.44 (s, 2H, pyrrole-H), 2.45 (s, 6H, -SMe). ^{13}C NMR (126 MHz, $CDCl_3$) δ 160.7, 136.7, 135.5, 130.5, 129.9, 129.1, 126.1, 116.1, 116.0, 110.0, 15.7. HRMS (ESI^+) m/z calcd for $C_{24}H_{21}FNS_2$: 406.1094 $[M]^+$; found 406.1094.

1.5 Synthesis of 4-(2,5-bis(4-(methylthio)phenyl)-1H-pyrrol-1-yl)benzaldehyde (**BTPP-CHO**)

Following the general procedure for **BTPP-NMe$_2$**, reaction of 4-(2,5-dibromo-1H-pyrrol-1-yl)benzaldehyde (250.0 mg, 0.76 mmol), MTPBA (280.9 mg, 1.67 mmol), $Pd(PPh_3)_4$ (46.2 mg, 0.04 mmol), and K_2CO_3 (314.6 mg, 2.28 mmol) afforded **BTPP-CHO** as an orange-yellow solid (268.5 mg, 0.65 mmol, 85% yield). m.p. 168–169 °C. ^{1}H NMR (500 MHz, $CDCl_3$) δ 9.99 (s, 1H, -CHO), 7.77 (d, *J* = 8.3 Hz, 2H, phenyl-H), 7.15 (d, *J* = 8.3 Hz, 2H, phenyl-H), 7.06 (d, *J* = 8.3 Hz, 4H, phenyl-H), 6.94 (d, *J* = 8.4 Hz, 4H, phenyl-H), 6.46 (s, 2H, pyrrole-H), 2.44 (s, 6H, -SMe). ^{13}C NMR (126 MHz, $CDCl_3$) δ 191.4, 144.2, 137.2, 135.3, 134.8, 130.4, 129.5, 129.5, 129.3, 126.1, 110.9, 15.7. HRMS (ESI^+) m/z calcd for $C_{25}H_{23}NOS_2$: 416.1137 $[M]^+$; found 416.1138.

1.6 Synthesis of ethyl 4-(2,5-bis(4-(methylthio)phenyl)-1H-pyrrol-1-yl)benzoate (**BTPP-COOEt**)

Following the general procedure for **BTPP-NMe$_2$**, reaction of ethyl 4-(2,5-dibromo-1H-pyrrol-1-yl)benzoate (250.0 mg, 0.67 mmol), MTPBA (247.7 mg, 1.47 mmol), $Pd(PPh_3)_4$ (46.2 mg, 0.04 mmol), and K_2CO_3 (277.4 mg, 2.01 mmol) afforded **BTPP-COOEt** as a white solid (252.5 mg, 0.55 mmol, 82% yield). m.p. 205–206 °C. ^{1}H NMR (500 MHz, $CDCl_3$) δ 7.93 (d, *J* = 8.4 Hz, 2H, phenyl-H), 7.14–7.01 (m, 6H, phenyl-H), 6.94 (d, *J* = 8.3 Hz, 4H, phenyl-H), 6.45 (s, 2H, pyrrole-H), 4.46–4.26 (m, 2H, -CH_2-), 2.44 (s, 6H, -SMe), 1.39 (t, *J* = 7.1 Hz, 3H, -Me). ^{13}C NMR (126 MHz, $CDCl_3$) δ 166.1, 142.9, 136.9, 135.3, 130.4, 129.7, 129.3, 129.2, 128.8, 126.1, 110.6, 61.4, 15.7, 14.4. HRMS (ESI^+) m/z calcd for $C_{27}H_{25}NO_2S_2$: 480.1399 $[M]^+$; found 480.1400.

2. NMR characterization

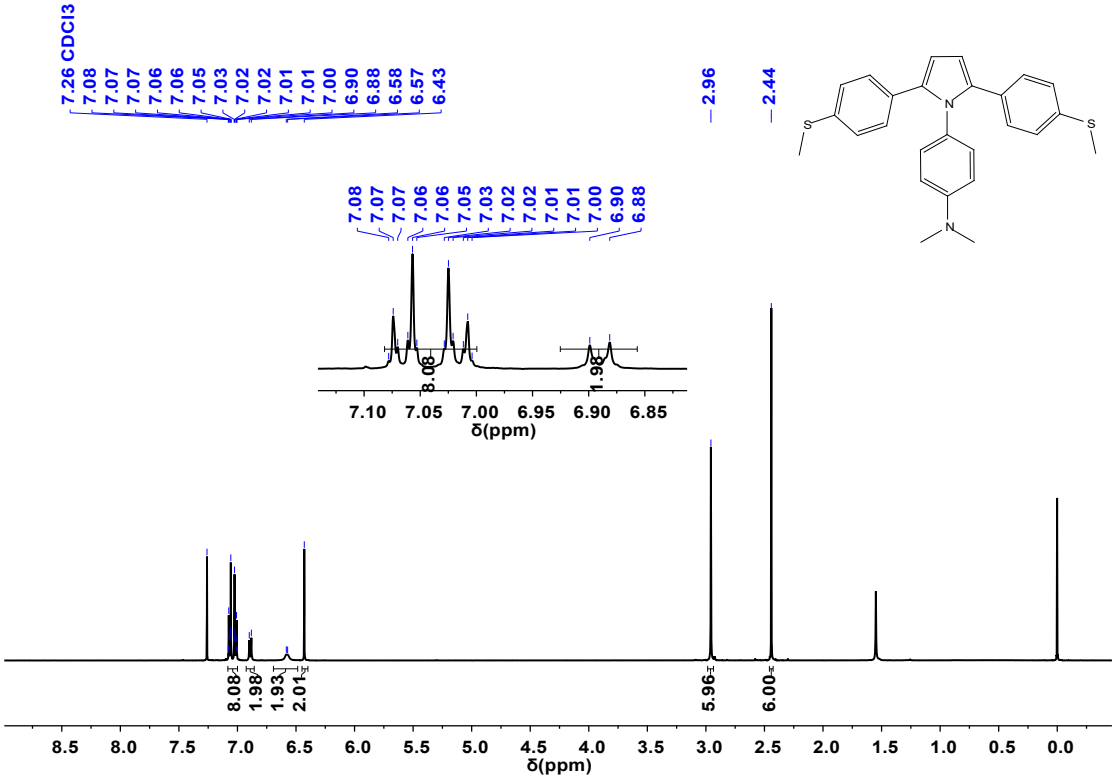

Fig. S1 ^{1}H NMR spectrum of **BTPP-NMe$_2$** in $CDCl_3$.

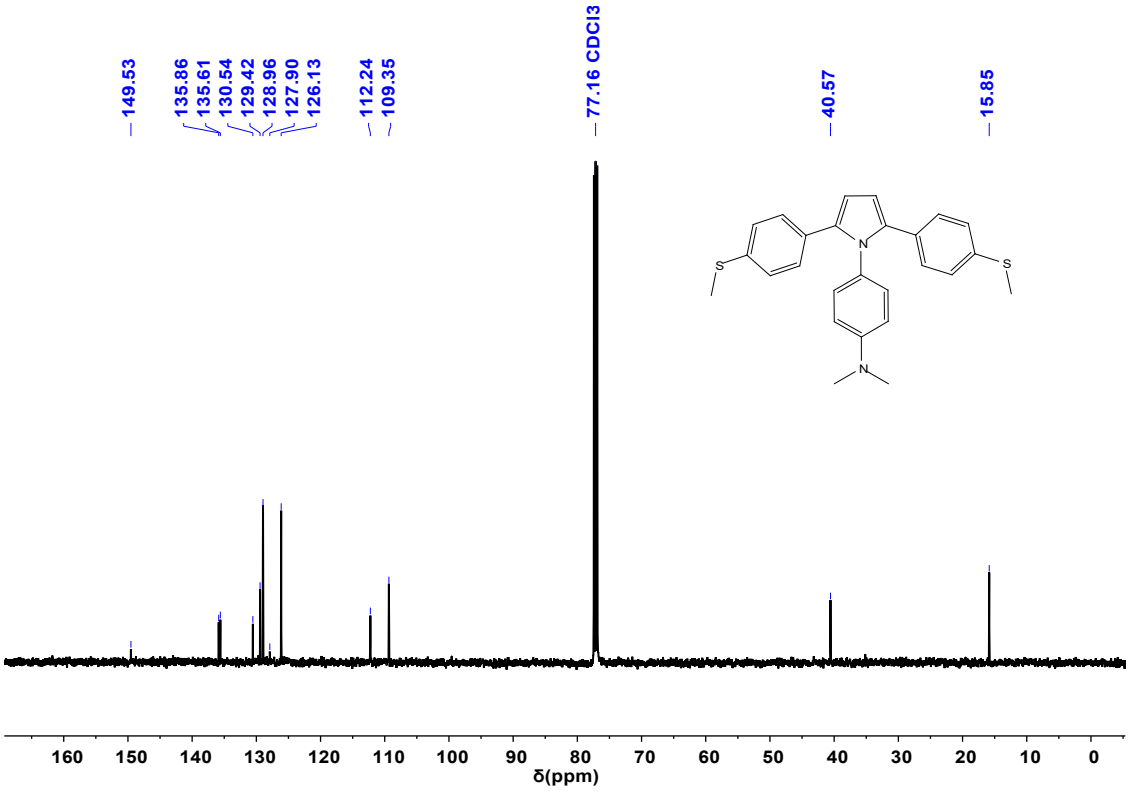

Fig. S2 ^{13}C NMR spectrum of **BTPP-NMe_2** in $CDCl_3$.

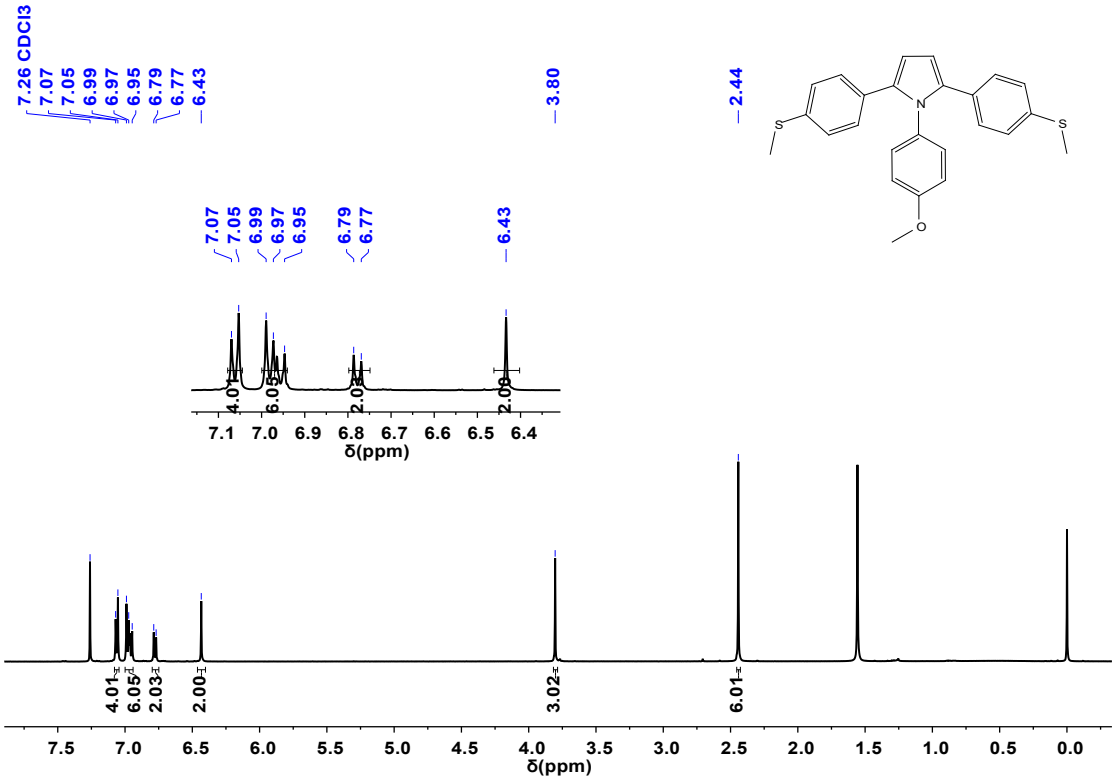

Fig. S3 ^{1}H NMR spectrum of **BTPP-OMe** in $CDCl_3$.

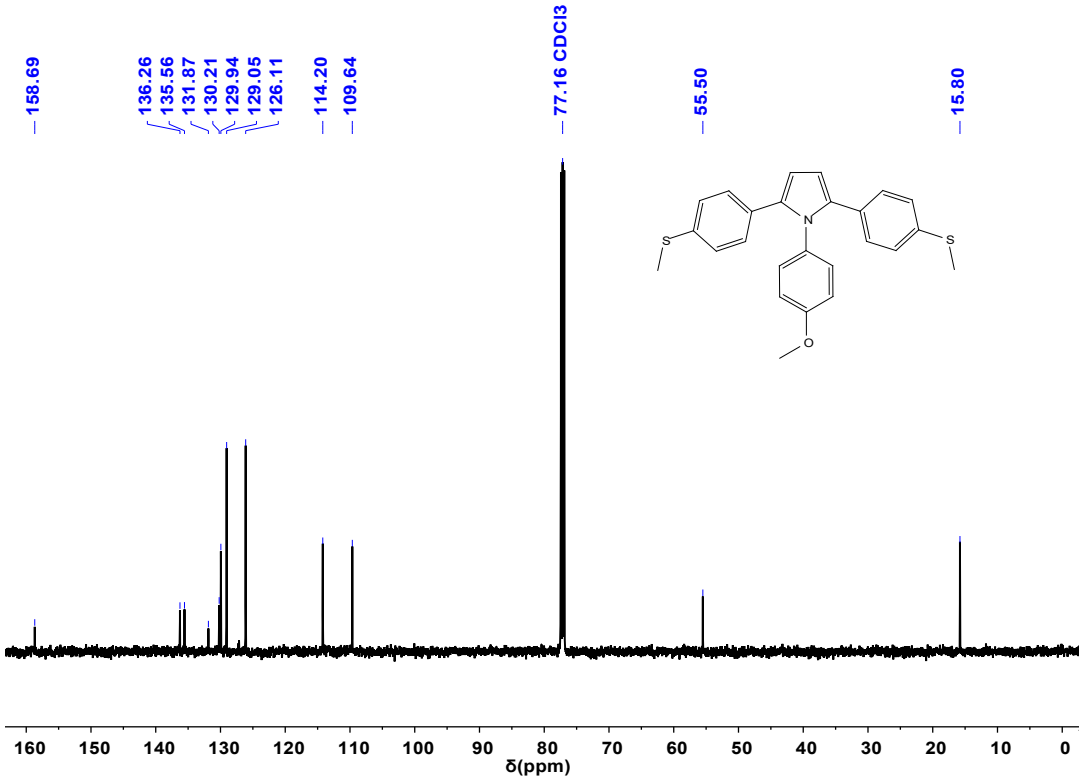

Fig. S4 ^{13}C NMR spectrum of **BTPP-OMe** in $CDCl_3$.

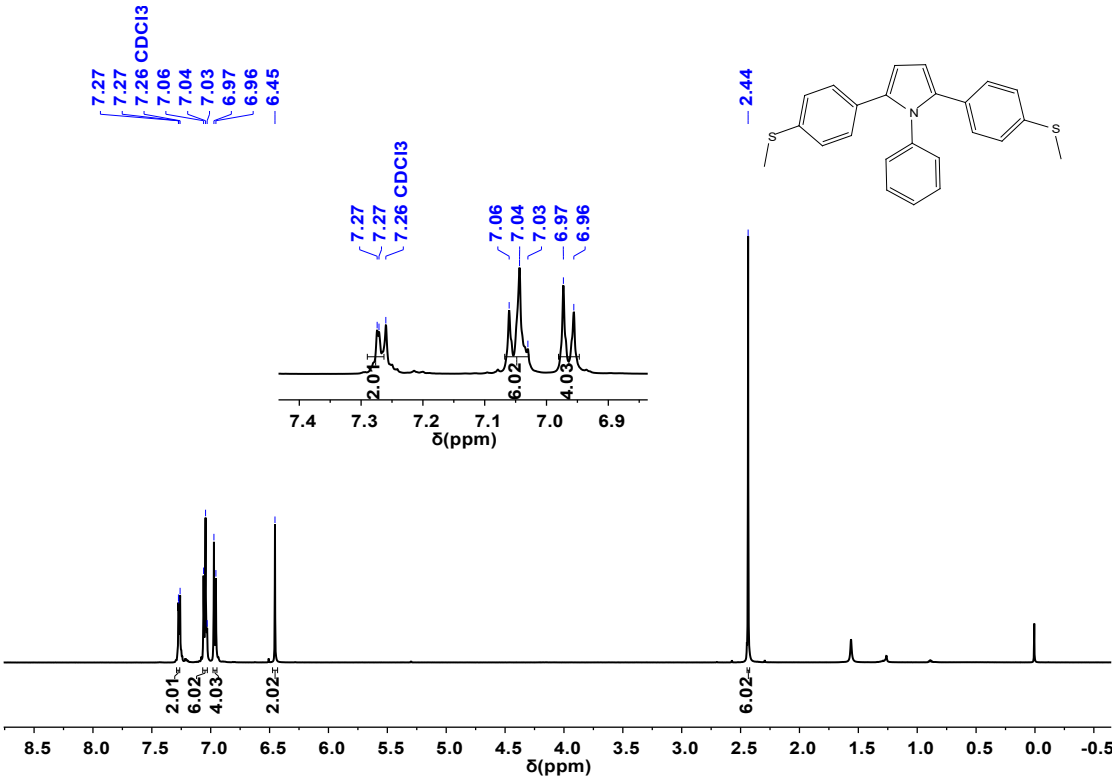

Fig. S5 ^{1}H NMR spectrum of **BTPP-H** in $CDCl_3$.

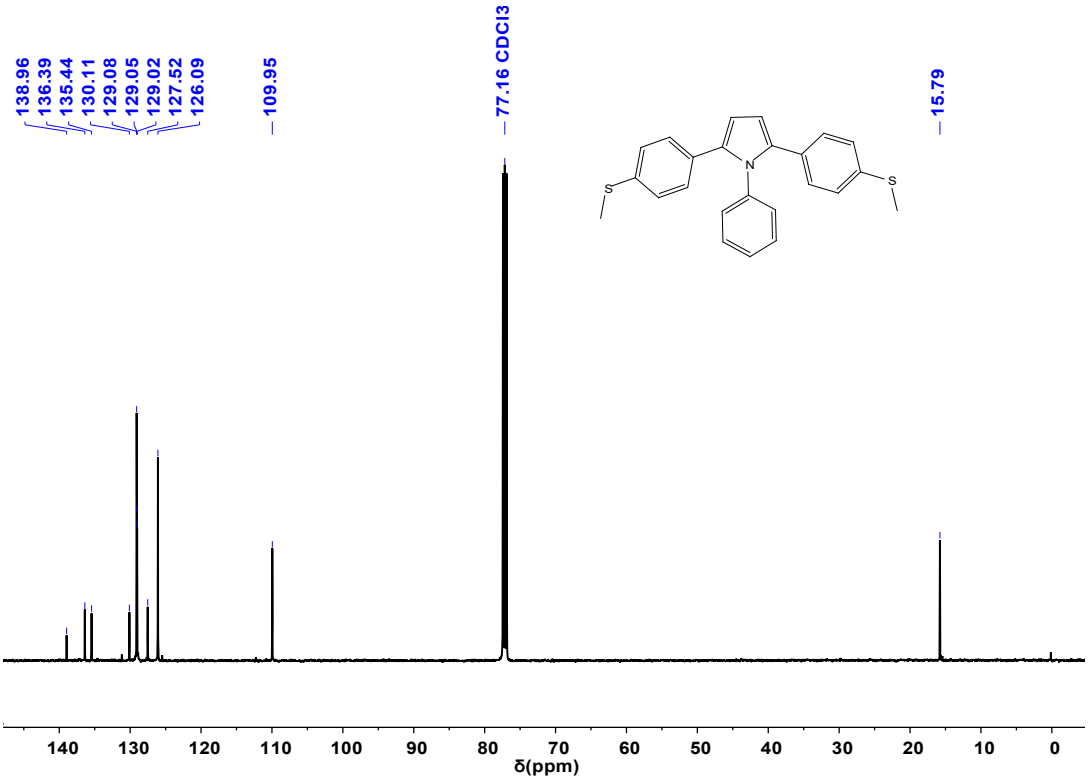

Fig. S6 ^{13}C NMR spectrum of **BTPP-H** in $CDCl_3$.

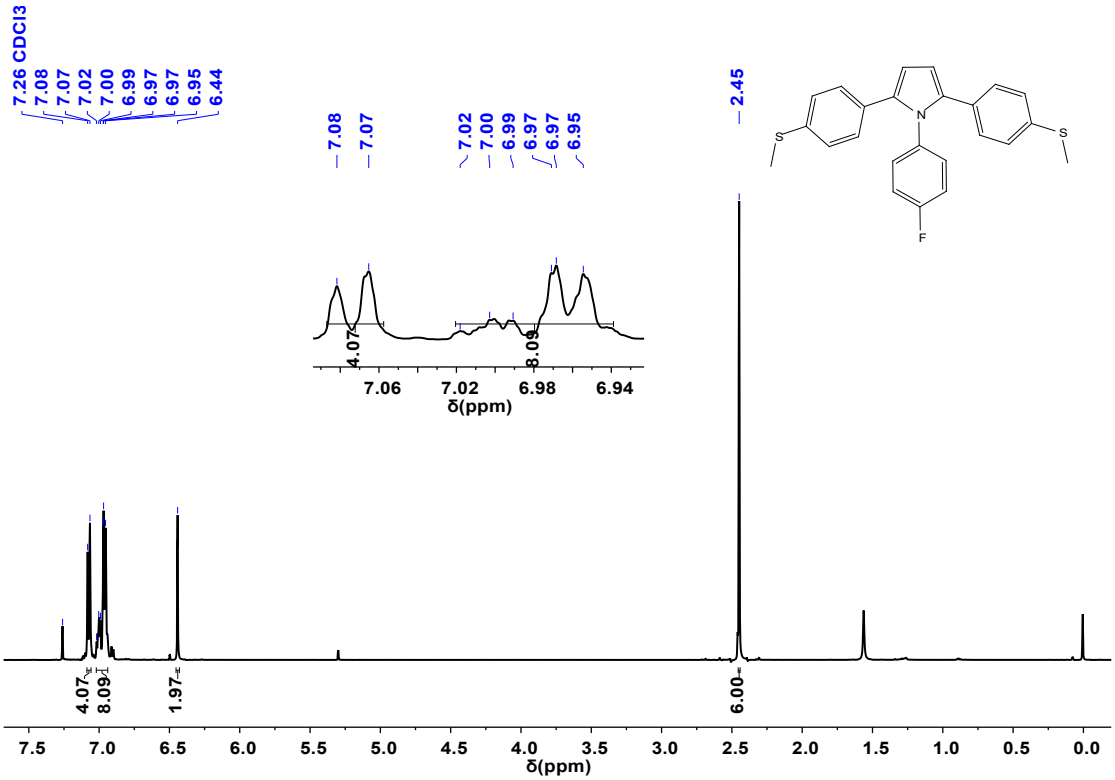

Fig. S7 ^{1}H NMR spectrum of **BTPP-F** in $CDCl_3$.

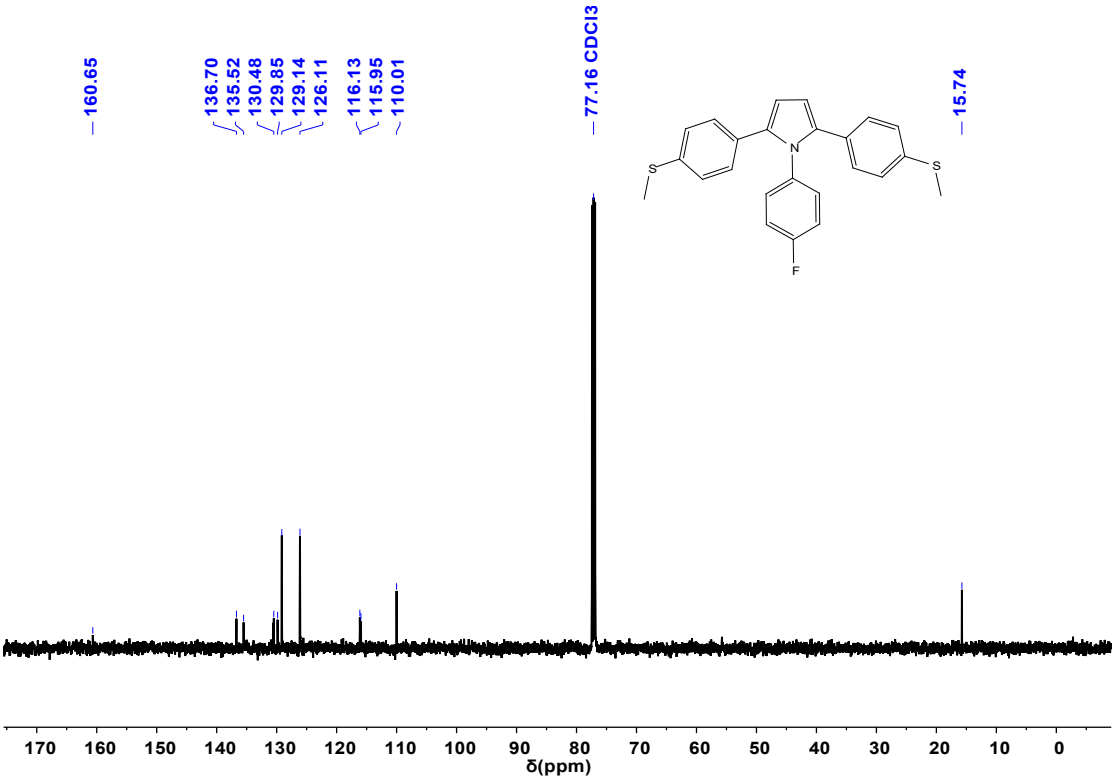

Fig. S8 ^{13}C NMR spectrum of **BTPP-F** in $CDCl_3$.

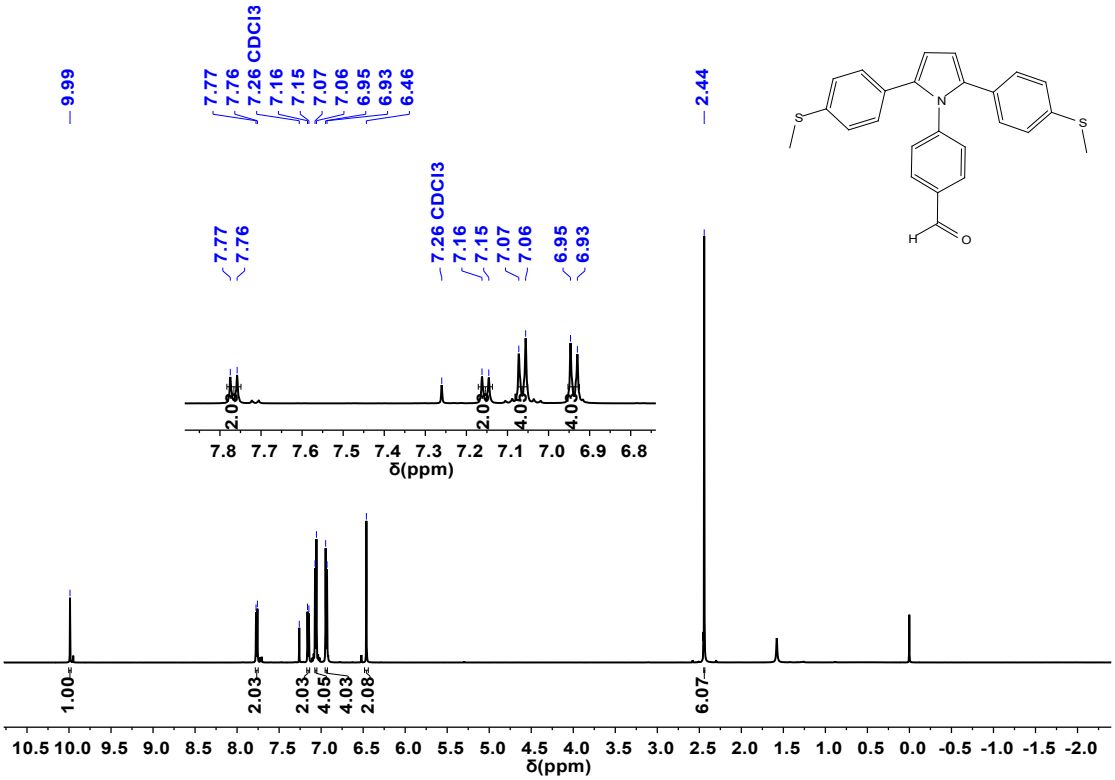

Fig. S9 ^{1}H NMR spectrum of **BTPP-CHO** in $CDCl_3$.

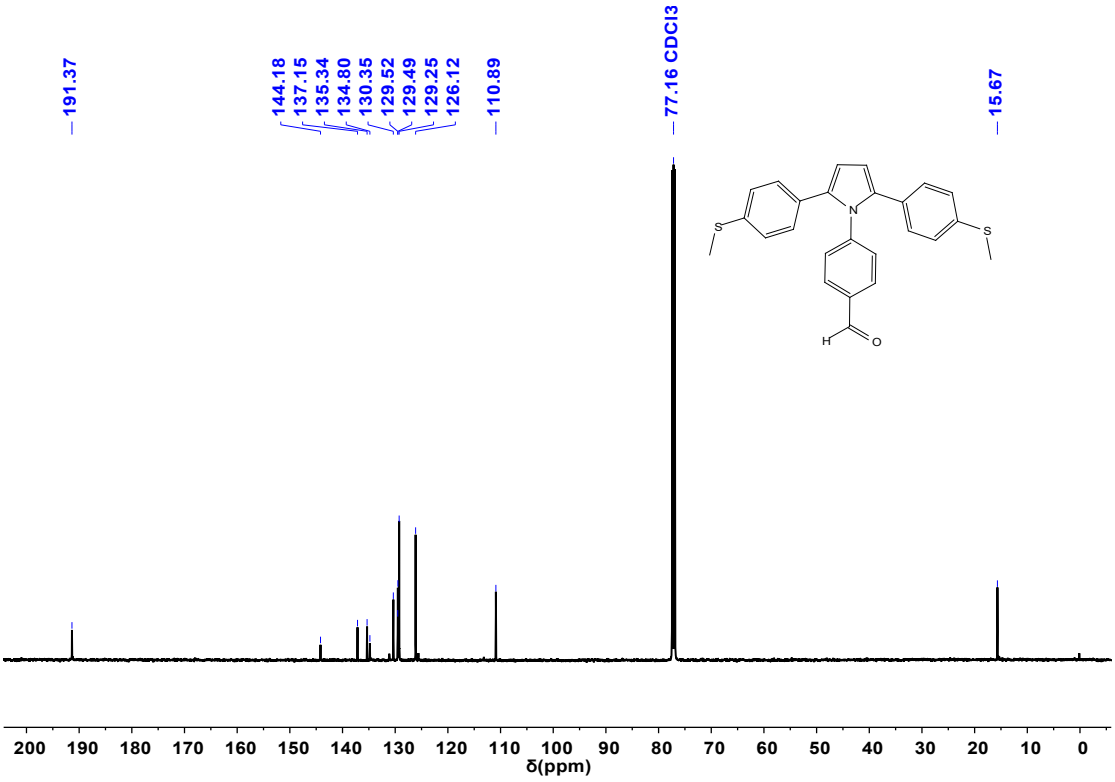

Fig. S10 ^{13}C NMR spectrum of **BTPP-CHO** in $CDCl_3$.

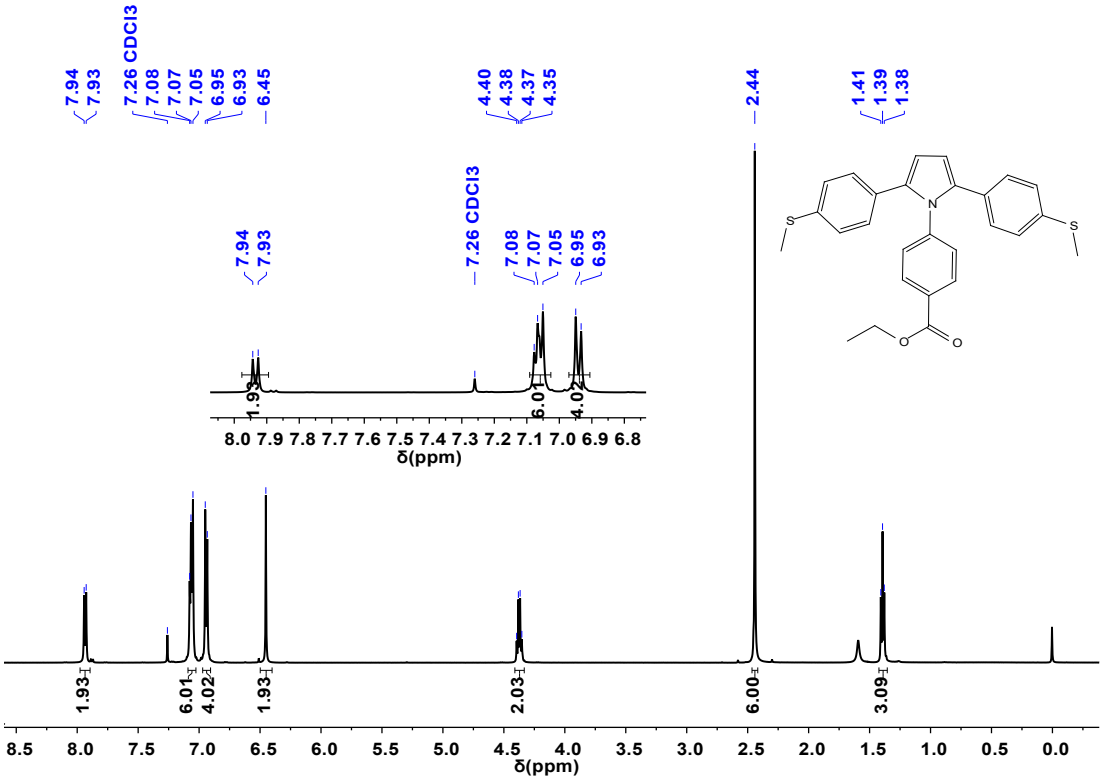

Fig. S11 ^{1}H NMR spectrum of **BTPP-COOEt** in $CDCl_3$.

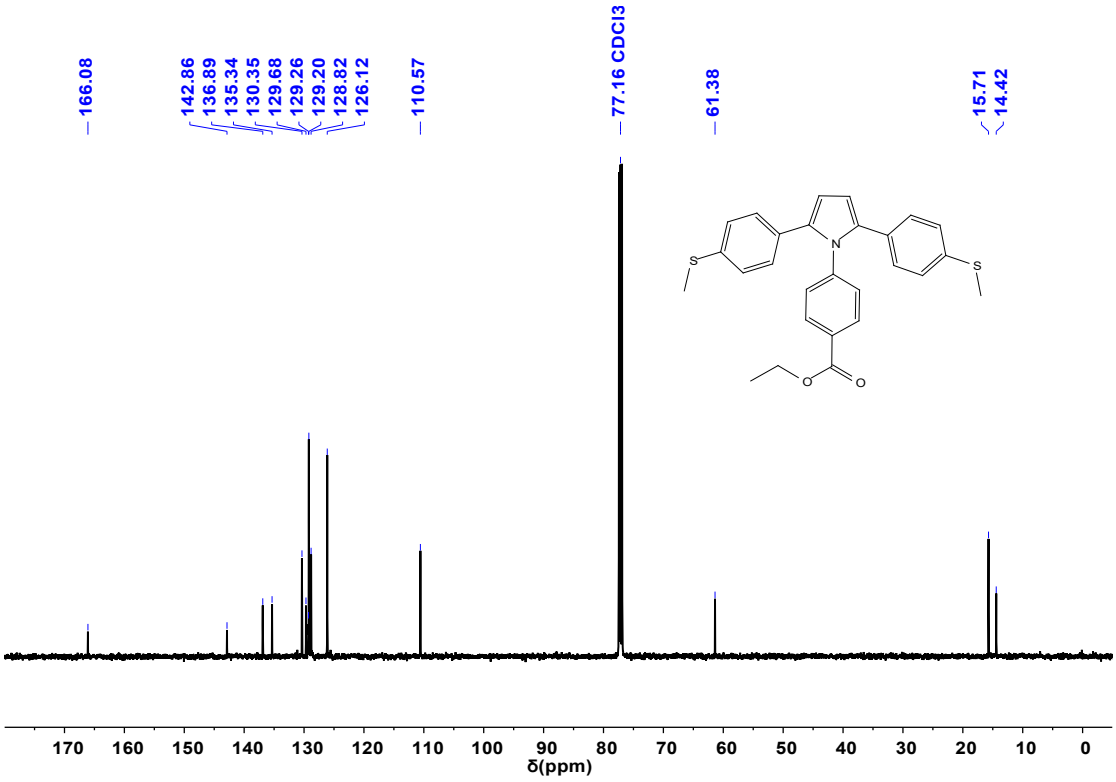

Fig. S12 ^{13}C NMR spectrum of **BTPP-COOEt** in $CDCl_3$.

3. HRMS characterization

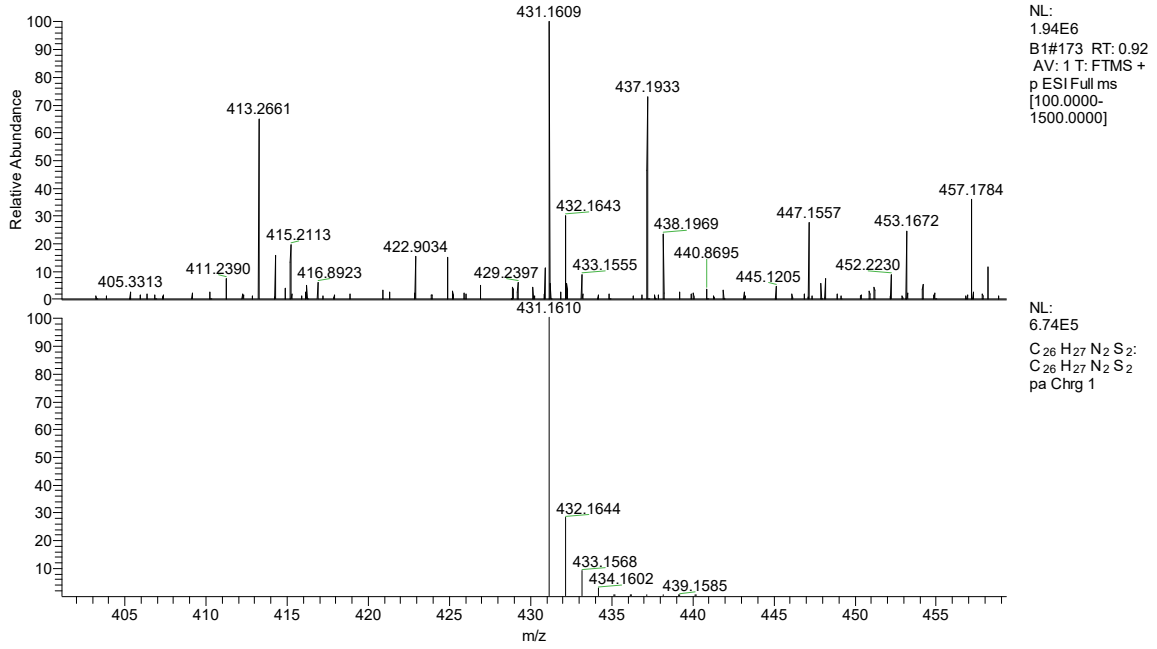

Fig. S13 HRMS of **BTPP-NMe$_2$**.

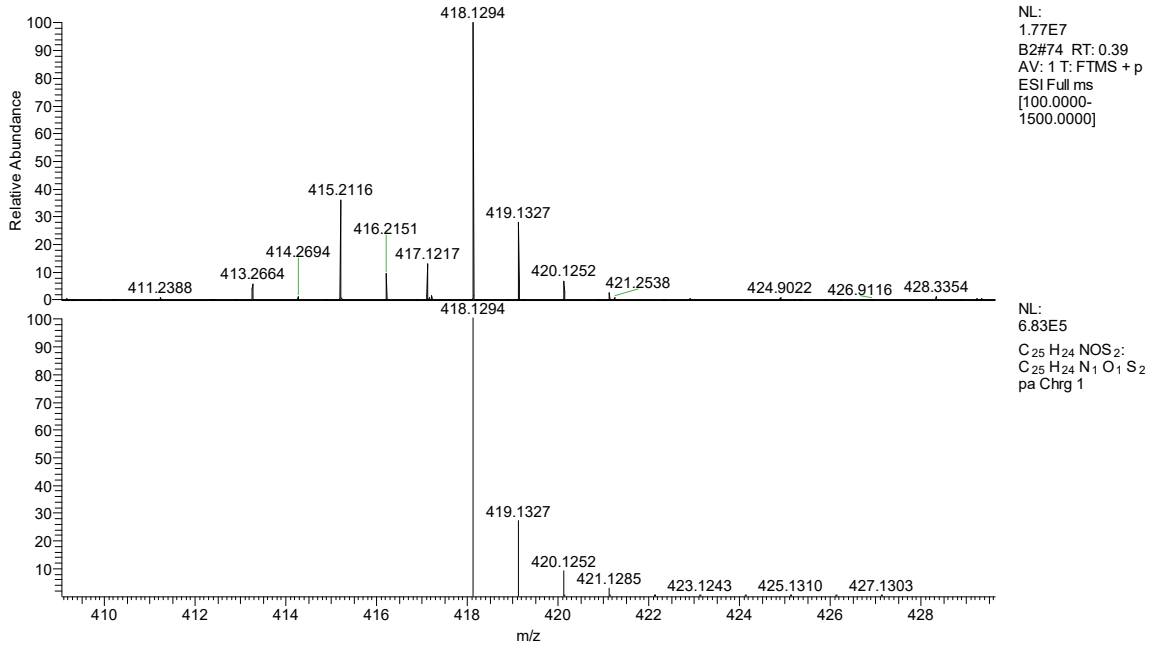

Fig. S14 HRMS of **BTPP-OMe**.

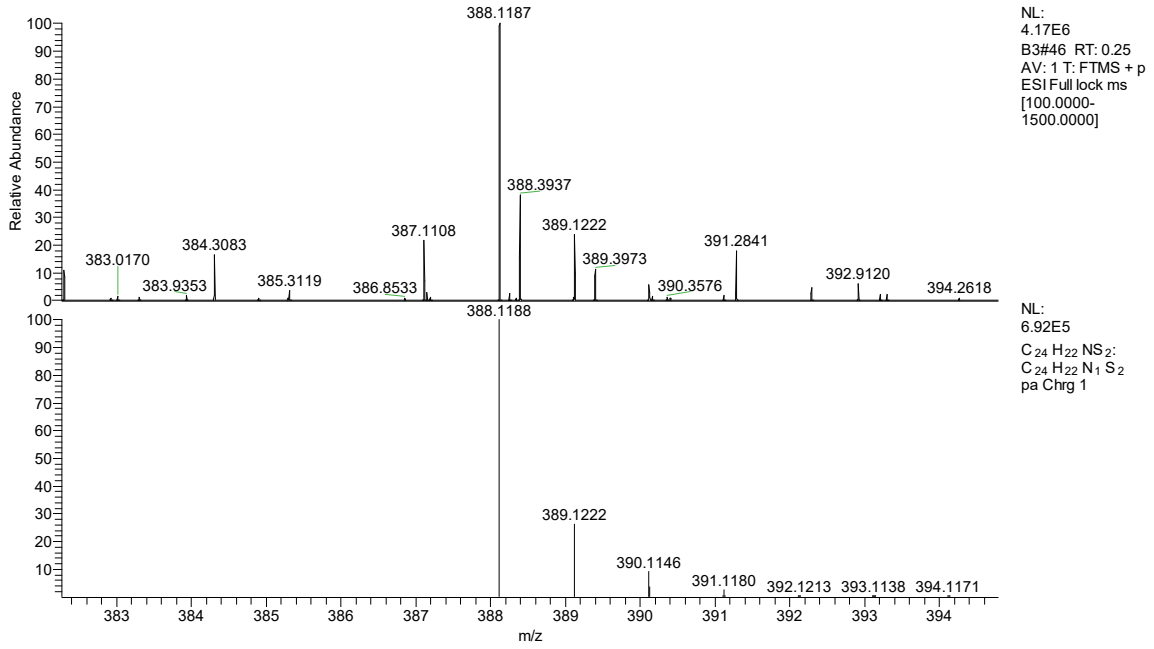

Fig. S15 HRMS of **BTPP-H**.

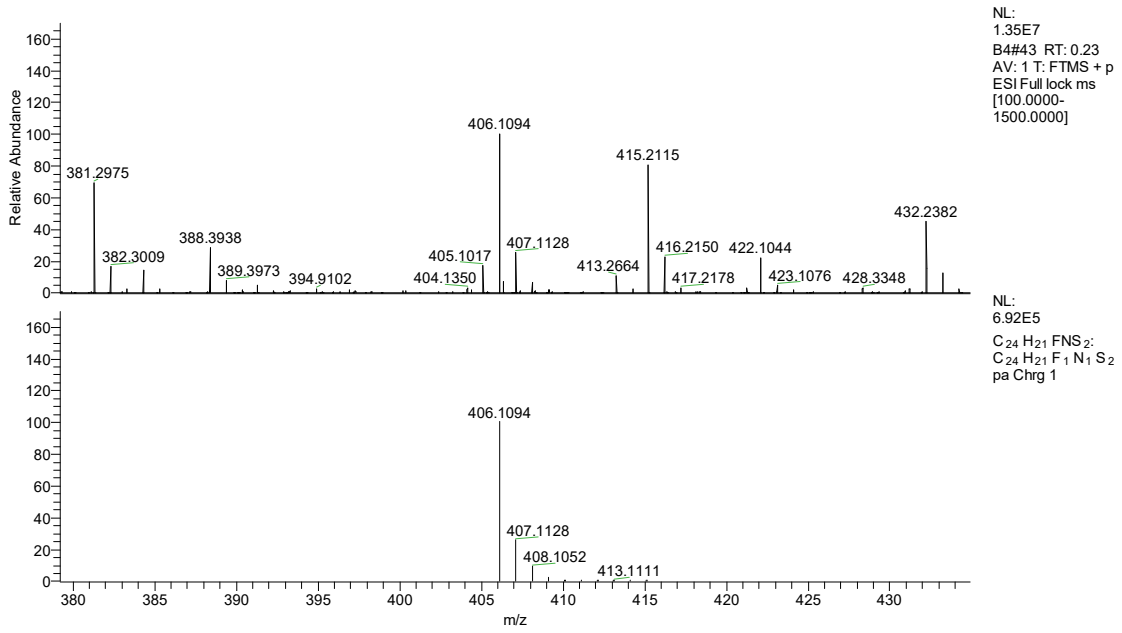

Fig. S16 HRMS of **BTPP-F**.

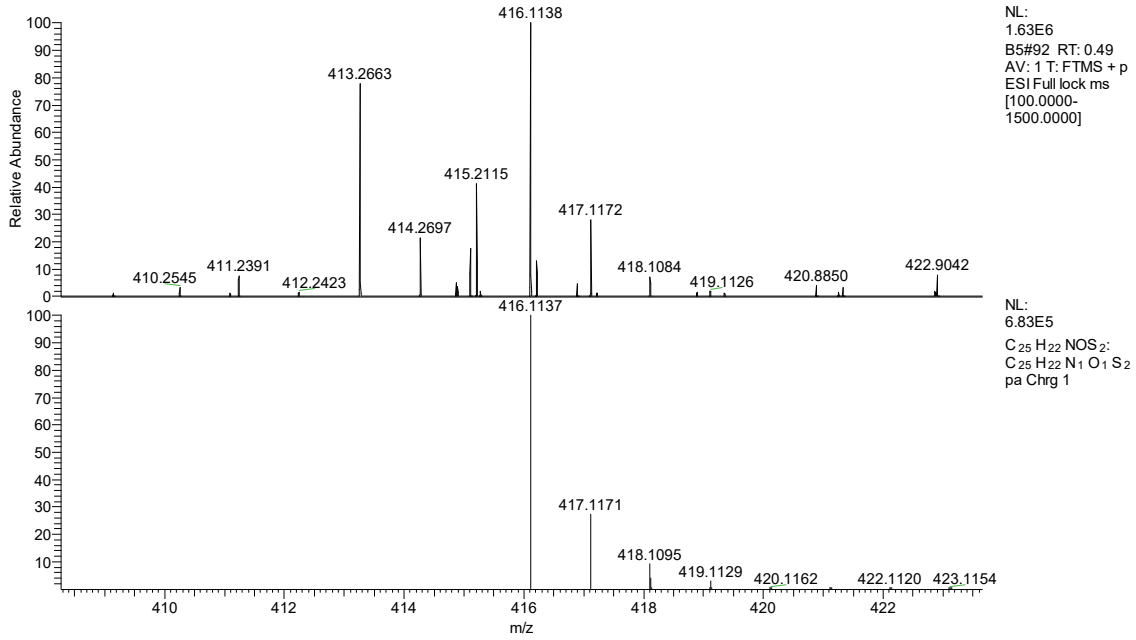

Fig. S17 HRMS of **BTPP-CHO**.

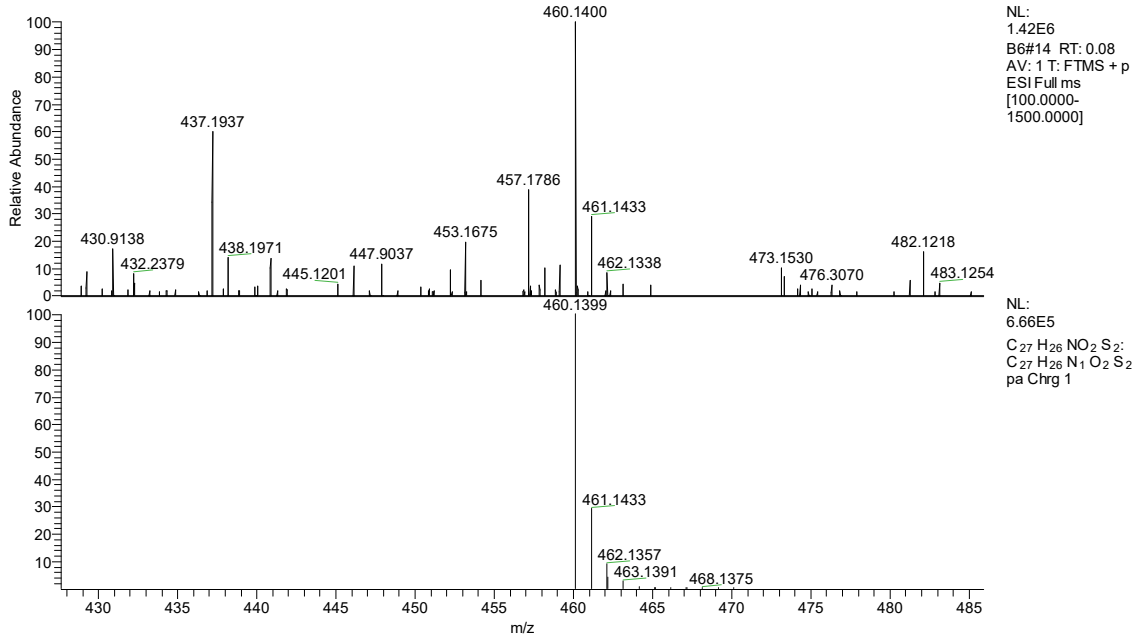

Fig. S18 HRMS of **BTPP-COOEt**.

4. IR spectroscopy

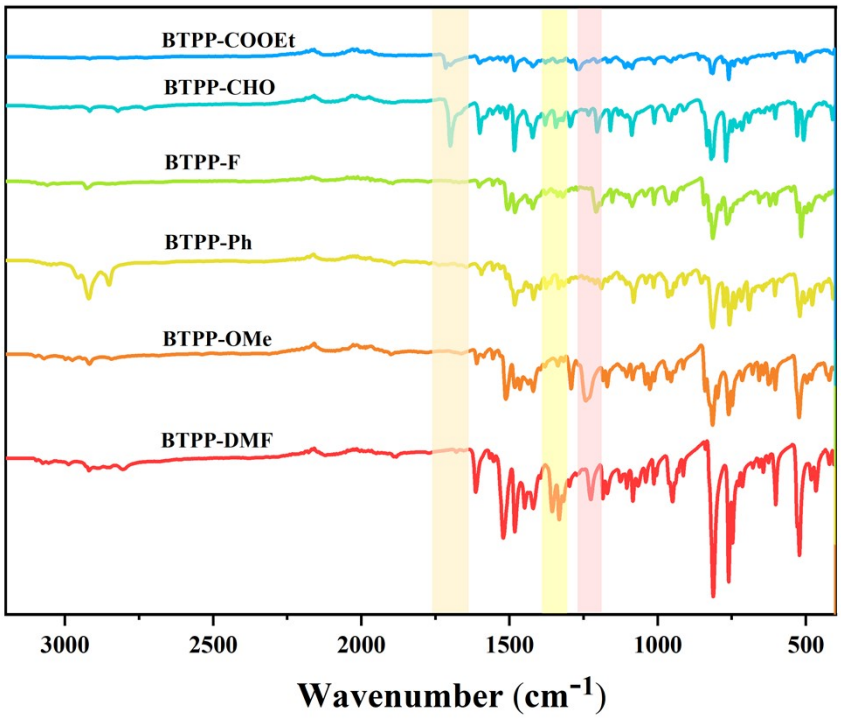

Fig. S19 Infrared spectra of **BTPP** derivatives recorded using KBr pellet technique in the range of 4000–400 cm^{-1}.

Table S1. Significant IR absorption peaks for **BTPP** derivatives.

Compound	Wavenumber (cm^{-1})
BTPP-NMe_2	1014.1, 1522.0, 1482.5, 1450.0, 1420.8, 1357.2, 1332.6, 1225.5, 1084.3, 1013.4, 950.3, 812.4, 761.3, 602.2, 522.1
BTPP-OMe	1512.9, 1418.9, 1292.1, 1241.5, 1170.6, 1027.0, 955.1, 815.3, 760.8, 603.6, 523.6
BTPP-H	1483.0, 1419.8, 1081.4, 962.8, 814.8, 758.4, 692.3, 602.5, 520.7, 478.7
BTPP-F	1510.5, 1481.5, 1422.2, 1210.1, 1154.2, 1086.2, 1011.5, 959.9, 815.3, 788.0, 516.3
BTPP-CHO	1701.9, 1601.1, 1484.9, 1424.7, 1381.3, 1344.6, 1296.9, 1205.8, 1160.0, 1089.1, 1012.9, 960.4, 820.6, 768.5, 532.8, 506.7
BTPP-COOEt	1717.8, 1605.4, 1484.9, 1421.8, 1274.7, 1112.2, 1084.8, 817.2, 761.3, 530.8, 508.6

5. Theoretical calculations

5.1 Frontier molecular orbitals

All calculations were performed using the Gaussian 16 software package with the B3LYP-D3(BJ) functional and 6-31G(d) basis set. Geometry optimization and frequency calculations were carried out for all compounds to confirm no imaginary frequencies.

Table S2. Calculated HOMO and LUMO Energy Levels (in eV) and HOMO–LUMO Gaps for **BTPP** derivatives.

	BTPP-NMe_2	**BTPP-OMe**	**BTPP-H**	**BTPP-F**	**BTPP-CHO**	**BTPP-COOEt**
HOMO (eV)	−5.020	−4.930	−4.983	−4.906	−4.940	−4.941
LUMO (eV)	−0.917	−0.811	−0.870	−0.736	−1.920	−1.459
Gap (eV)	4.103	4.120	4.113	4.170	3.020	3.482

5.2 Comparison of dihedral angles determined from DFT

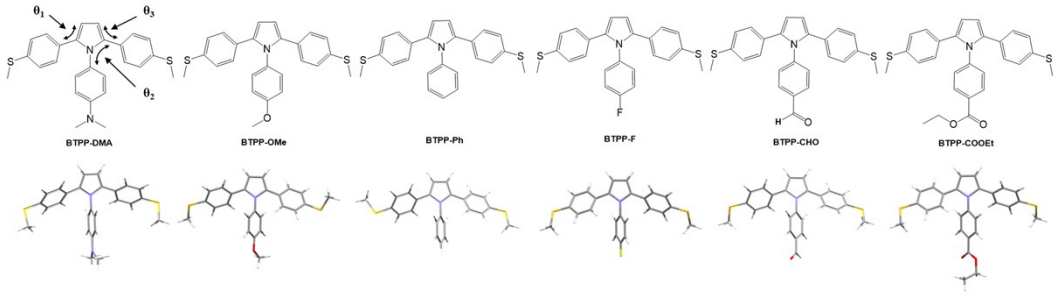

Fig. S20 Molecular structures of **BTPP** derivatives with dihedral-angle definitions. The dihedral angles θ_1–θ_3 are defined on the pyrrole, applicable to all derivatives, representing in sequence the torsion between the substituents at positions 5, 1, and 2 and the core five-membered ring. Top row: chemical structures with the defined dihedral angles θ_1–θ_3 indicated. Bottom row: geometrically optimized structures.

Table S3. Comparison of DFT B3LYP/6-31G(d) dihedral angles for the rings of **BTPP** derivatives.

Compound	θ_1 (°)	θ_2 (°)	θ_3 (°)
BTPP-NMe$_2$	39.3	89.5	39.0
BTPP-OMe	40.2	59.8	39.5
BTPP-H	40.8	58.6	40.0
BTPP-F	41.0	58.4	41.0
BTPP-CHO	42.6	54.9	42.4
BTPP-COOEt	41.7	56.0	41.8

5.3 NCI analysis of BTPP-NMe$_2$

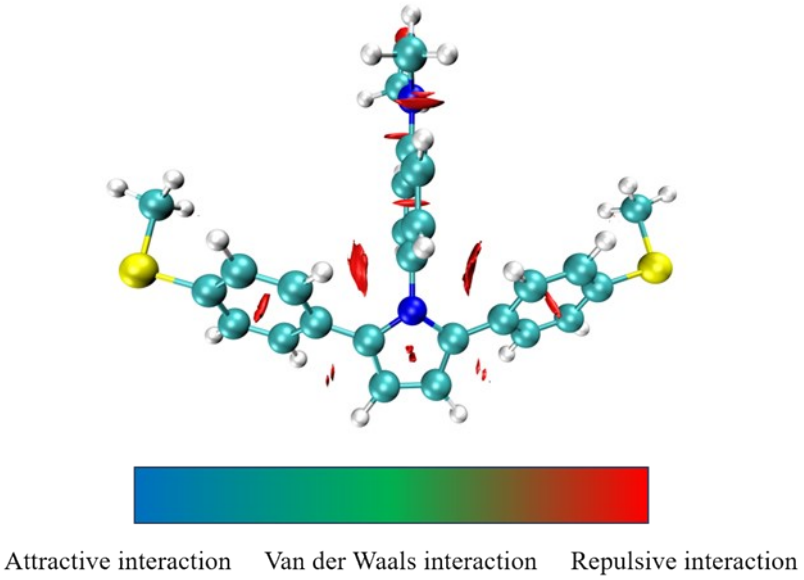

Fig. S21 NCI Analysis of **BTPP-NMe$_2$**

5.4 Calculation of Aromaticity Indices (NICS and ACID) for BTPP derivatives

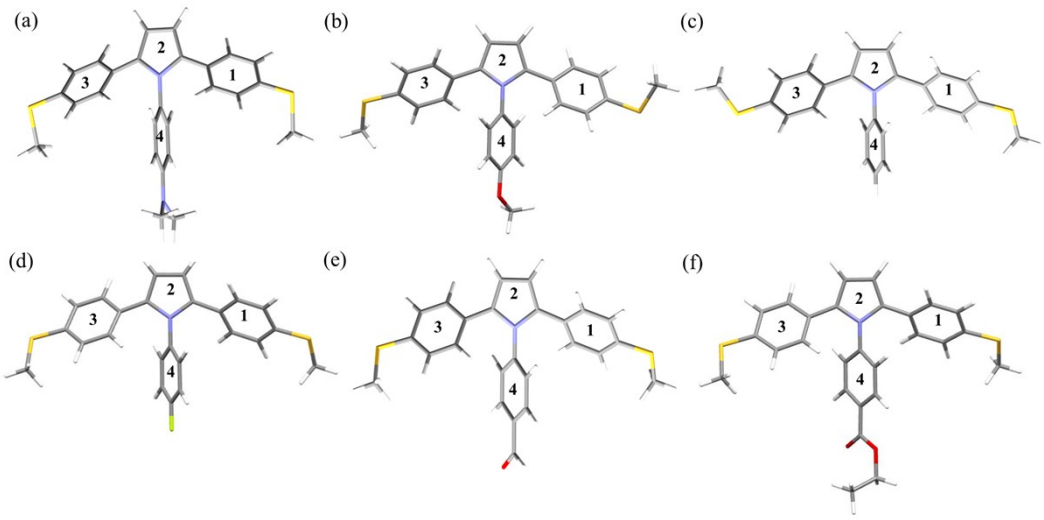

Fig. S22 Molecular Structure Diagrams of **BTPP** Derivatives from NICS Calculations (Labels 1, 2, 3, and 4 for Aromaticity of Different Benzene Rings)

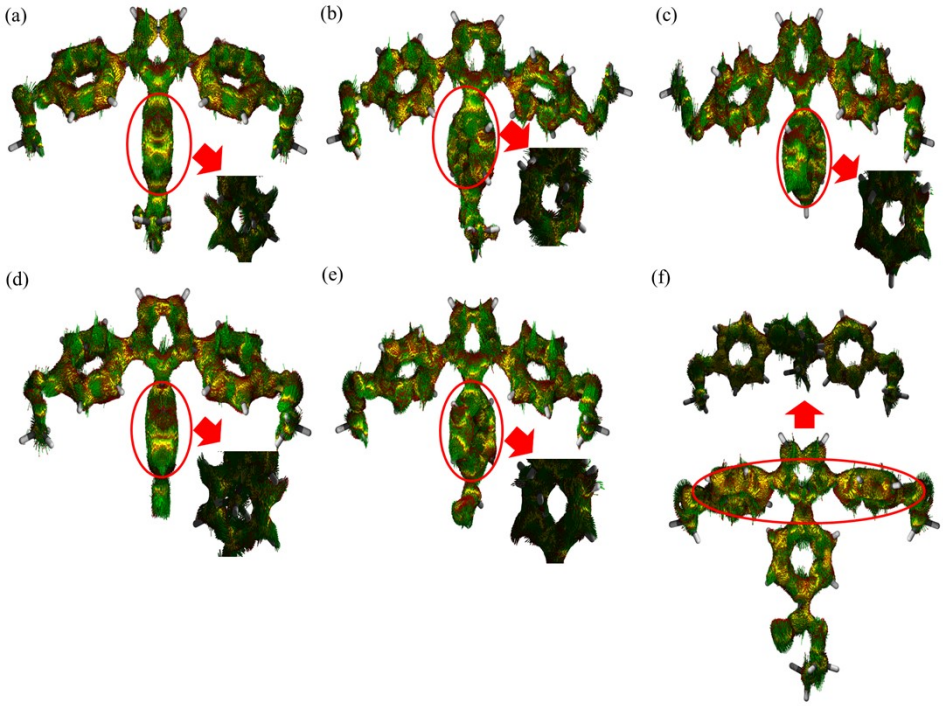

Fig. S23 ACID Current Density Distributions of **BTPP** Derivatives

Table S4. Comparison of NICS(0), NICS(+1)zz and NICS(-1)zz at Various Sites of **BTPP** derivatives. The positions 1-4 correspond to the rings labeled in Fig. S21. Negative NICS values indicate aromatic character.

		1	**2**	**3**	**4**
BTPP-NMe_2	NICS(0)	−6.7712	−18.7840	−6.7900	−6.1047
	NICS(+1)zz	−12.9519	−19.0957	−12.6671	−3.4859
	NICS(-1)zz	−13.4381	−19.1460	−13.1054	−3.8784
		1	**2**	**3**	**4**
BTPP-OMe	NICS(0)	−7.5897	−16.9480	−7.4933	−4.2963
	NICS(+1)zz	−12.6207	−19.4468	−15.6010	−6.5122
	NICS(-1)zz	−13.3022	−18.9715	−15.3250	−6.9181
		1	**2**	**3**	**4**
BTPP-H	NICS(0)	−7.5495	−17.2121	−7.7167	−3.5922
	NICS(+1)zz	−15.2336	−19.3625	−13.0197	−7.2005
	NICS(-1)zz	−14.8804	−18.9999	−13.8609	−7.3436
		1	**2**	**3**	**4**
BTPP-F	NICS(0)	−7.4876	−16.0455	−7.4884	−2.5925
	NICS(+1)zz	−14.1273	−19.2729	−14.4385	−7.4796
	NICS(-1)zz	−14.4421	−19.2736	−14.1239	−7.4791
		1	**2**	**3**	**4**
BTPP-CHO	NICS(0)	−7.4119	−16.3091	−7.5178	−4.1957
	NICS(+1)zz	−14.6130	−18.6752	−12.9321	−8.1847
	NICS(-1)zz	−14.1825	−18.8731	−13.4009	−8.1143
		1	**2**	**3**	**4**
BTPP-COOEt	NICS(0)	−7.4839	−15.9659	−7.3477	−5.6871
	NICS(+1)zz	−15.0035	−18.9039	−12.5940	−7.2398
	NICS(-1)zz	−15.3631	−18.5113	−12.0571	−7.2568

5.5 Molecular Electrostatic Potential (MEP) of pyrrole-based compounds

Molecular electrostatic potential (MEP) surfaces were mapped onto the electron density isosurface (0.001 e bohr^{-3}) using the same DFT-optimized geometries.

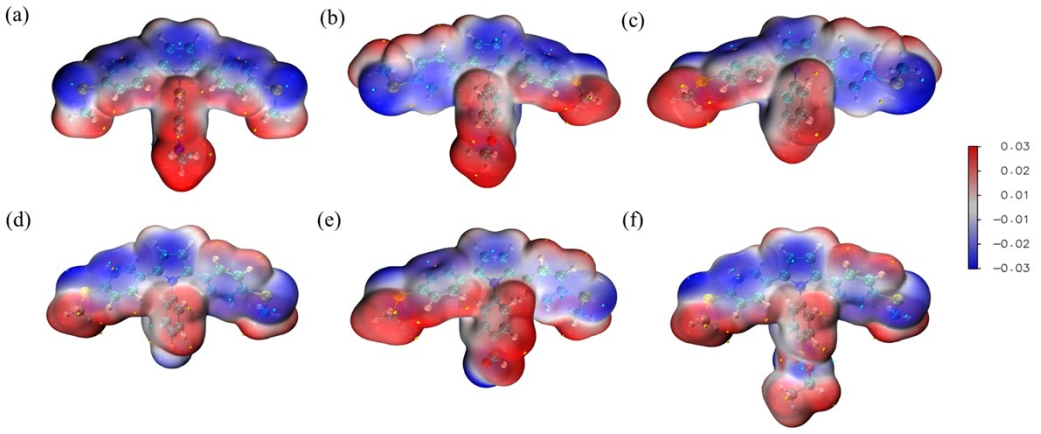

Fig. S24 Molecular electrostatic potential (MEP) surfaces of (a) **BTPP-NMe$_2$** (b) **BTPP-OMe** (c) **BTPP-H** (d) **BTPP-F** (e) **BTPP-CHO** and (f) **BTPP-COOEt**. Color scale: blue (negative, electron-rich) to red (positive, electron-deficient).

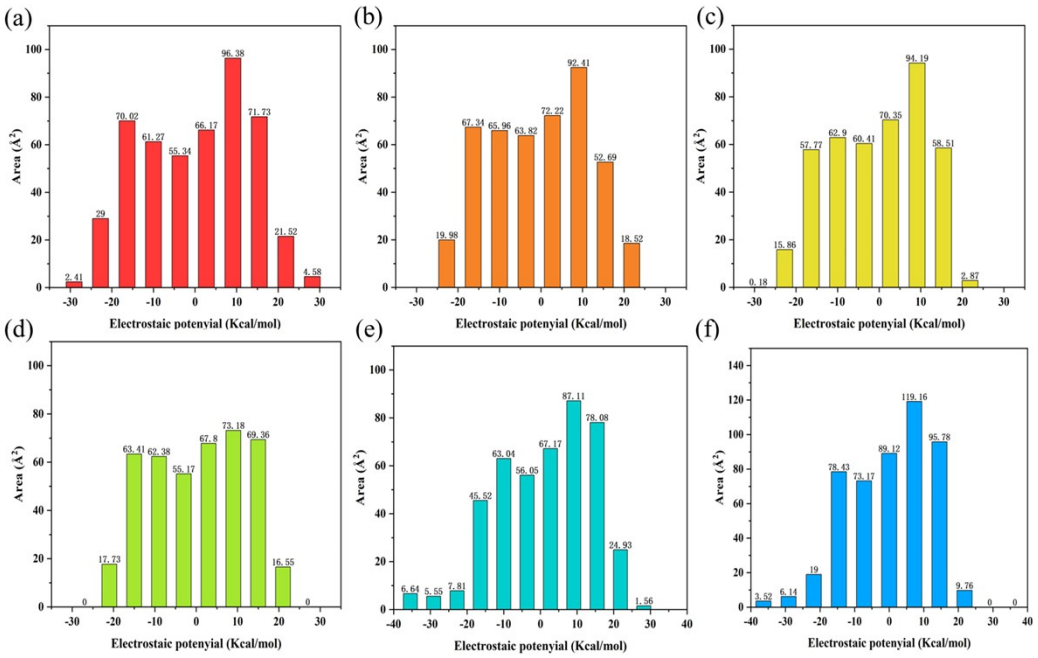

Fig. S25 Statistical distribution of the relative area covered by negative (blue) and positive (red) electrostatic potential regions for (a) **BTPP-NMe$_2$** (b) **BTPP-OMe** (c) **BTPP-H** (d) **BTPP-F** (e) **BTPP-CHO** and (f) **BTPP-COOEt**.

6. UV-vis absorption spectroscopy and extinction coefficients

Table S5. Absorption maxima and extinction coefficients for UV-vis spectra of **BTPP** derivatives, λ_{max} reported in nm, and ε in M^{-1} cm^{-1}.

Compound	λ_1	ε_1	λ_2	ε_2
BTPP-NMe_2	264	15184	324	22145
BTPP-OMe	253	18608	320	56186
BTPP-H	253	16986	323	49791
BTPP-F	253	20504	319	60091
BTPP-CHO	271	51092	308	80634
BTPP-COOEt	265	23333	314	35727

7. BTPP derivatives Excited State Data Calculated by TD-DFT

Table S6. Specific data of the top 10 excited states of **BTPP-NMe_2** obtained from TD-DFT calculations.

Excited state	Excitation energy (eV)	Calculate wavelength (nm)	Oscillator Strength (f)	Main orbital contributions (coefficient ≥ 0.1)	Transition Assignment (Corresponding to Orbital Number: HOMO=114，LUMO=115）
S_1	3.6241	342.11	1.1140	114→115 (0.702)	HOMO → LUMO
S_2	3.6949	335.55	0.0068	113→115 (0.704)	HOMO-1 → LUMO
S_3	4.2282	293.23	0.0298	114→116 (0.676), 114→119 (-0.146)	HOMO → LUMO+1, +4
S_4	4.3045	288.04	0.0084	114→117 (0.678), 108→115 (0.126)	HOMO → LUMO+2, HOMO-6 → LUMO
S_5	4.3122	287.52	0.0136	113→116 (0.661), 113→117 (0.137), 113→119 (-0.156)	HOMO-1 → LUMO+1, +2, +4
S_6	4.3595	284.40	0.0013	114→118 (0.676), 107→115 (-0.108), 109→115 (-0.111)	HOMO → LUMO+3, HOMO-7 → LUMO, HOMO-5 → LUMO
S_7	4.4134	280.92	0.0027	112→115 (0.647), 111→116 (-0.224)	HOMO-2 → LUMO, HOMO-3 → LUMO+1
S_8	4.4491	278.67	0.0019	114→119 (0.668), 114→116 (0.130), 114→117 (-0.111)	HOMO → LUMO+4, +1, +2
S_9	4.4800	276.75	0.0009	111→115 (0.641), 112→116 (-0.246)	HOMO-3 → LUMO, HOMO-2 → LUMO+1
S_{10}	4.5181	274.42	0.0252	113→117 (0.536), 113→119 (-0.368), 113→116 (-0.221)	HOMO-1 → LUMO+2, +4, +1

Table S7. Specific data of the top 10 excited states of **BTPP-OMe** obtained from TD-DFT calculations.

Excited state	Excitation energy (eV)	Calculate wavelength (nm)	Oscillator Strength (f)	Main orbital contributions (coefficient ≥ 0.1)	Transition Assignment (Corresponding to Orbital Number：HOMO=110，LUMO=111)
S1	3.6564	339.09	1.0627	110→111 (0.703)	HOMO → LUMO
S2	3.9867	310.99	0.0107	110→112 (0.693)	HOMO → LUMO+1
S3	4.2595	291.08	0.0089	110→114 (0.566), 110→113 (0.385)	HOMO → LUMO+3, HOMO → LUMO+2
S4	4.2898	289.02	0.0041	109→111 (0.569), 110→113 (0.283), 110→114 (-0.206), 108→111 (0.185)	HOMO-1 → LUMO, HOMO → LUMO+2, HOMO → LUMO+3, HOMO-2 → LUMO
S5	4.3321	286.20	0.0936	110→113 (0.451), 109→111 (-0.370), 110→114 (-0.302), 110→115 (0.154)	HOMO → LUMO+2, HOMO-1 → LUMO, HOMO → LUMO+3, HOMO → LUMO+4
S6	4.4576	278.14	0.0655	110→115 (0.465), 110→116 (0.396), 108→111 (-0.266), 107→111 (-0.136)	HOMO → LUMO+4, HOMO → LUMO+5, HOMO-2 → LUMO, HOMO-3 → LUMO
S7	4.4829	276.57	0.0139	110→116 (0.553), 110→115 (-0.401)	HOMO → LUMO+5, HOMO → LUMO+4
S8	4.5261	273.93	0.0348	108→111 (0.436), 107→111 (0.388), 110→115 (0.255), 110→113 (-0.167), 107→113 (0.118), 110→116 (0.114)	HOMO-2 → LUMO, HOMO-3 → LUMO, HOMO → LUMO+4, HOMO → LUMO+2, HOMO-3 → LUMO+2, HOMO → LUMO+5
S9	4.7028	263.64	0.0790	109→112 (0.627), 107→111 (0.146), 108→112 (0.122), 108→111 (-0.141)	HOMO-1 → LUMO+1, HOMO-3 → LUMO, HOMO-2 → LUMO+1, HOMO-2 → LUMO
S10	4.7860	259.05	0.0291	107→111 (0.487), 108→111 (-0.391), 109→112 (-0.180), 109→111 (0.128), 109→113 (-0.114)	HOMO-3 → LUMO, HOMO-2 → LUMO, HOMO-1 → LUMO+1, HOMO-1 → LUMO, HOMO-1 → LUMO+2

Table S8. Specific data of the top 10 excited states of **BTPP-H** obtained from TD-DFT calculations.

Excited state	Excitation energy (eV)	Calculated wavelength (nm)	Oscillator Strength (f)	Main orbital contributions (coefficient ≥ 0.1)	Transition Assignment (Corresponding to Orbital Number: HOMO=102，LUMO=103)
S1	3.6475	339.91	1.0048	102→103 (0.703)	HOMO → LUMO
S2	4.0385	307.00	0.0078	102→104 (0.688), 102→106 (0.117)	HOMO → LUMO+1, HOMO → LUMO+3
S3	4.0968	302.64	0.0586	102→105 (0.676), 102→106 (-0.171)	HOMO → LUMO+2, HOMO → LUMO+3
S4	4.3278	286.49	0.0697	102→106 (0.606)	HOMO → LUMO+3
S5	4.3711	283.65	0.0987	102→107 (0.635)	HOMO → LUMO+4
S6	4.4289	279.94	0.0028	101→103 (0.582)	HOMO-1 → LUMO
S7	4.5048	275.23	0.0096	102→108 (0.663)	HOMO → LUMO+5
S8	4.6897	264.38	0.0202	100→103 (0.494), 99→103 (0.390)	HOMO-2 → LUMO, HOMO-3 → LUMO
S9	4.8172	257.38	0.0786	99→103 (0.527), 100→103 (-0.319)	HOMO-3 → LUMO, HOMO-2 → LUMO
S10	4.8970	253.18	0.0511	101→104 (0.564)	HOMO-1 → LUMO+1

Table S9. Specific data of the top 10 excited states of **BTPP-F** obtained from TD-DFT calculations.

Excited state	Excitation energy (eV)	Calculate wavelength (nm)	Oscillator Strength (f)	Main orbital contributions (coefficient ≥ 0.1)	Transition Assignment (Corresponding to Orbital Number：HOMO=106，LUMO=107）
S_1	3.7070	334.46	1.0098	106→107 (0.703)	HOMO → LUMO
S_2	3.7856	327.52	0.0029	106→108 (0.703)	HOMO → LUMO+1
S_3	4.0896	303.17	0.1239	106→109 (0.697)	HOMO → LUMO+2
S_4	4.3168	287.21	0.0250	106→110 (0.583), 106→112 (0.331), 101→107 (-0.104), 105→107 (-0.139)	HOMO → LUMO+3, +5; HOMO-5 → LUMO; HOMO-1 → LUMO
S_5	4.3182	287.12	0.0877	106→111 (0.680), 102→107 (-0.108)	HOMO → LUMO+4; HOMO-4 → LUMO
S_6	4.4052	281.45	0.0026	106→112 (0.588), 106→110 (-0.300), 104→107 (0.130), 105→107 (0.172)	HOMO → LUMO+5, +3; HOMO-2 → LUMO; HOMO-1 → LUMO
S_7	4.5387	273.17	0.0068	105→107 (0.647), 104→107 (-0.182), 106→110 (0.167)	HOMO-1 → LUMO; HOMO-2 → LUMO; HOMO → LUMO+3
S_8	4.6242	268.12	0.0836	105→108 (0.678), 104→108 (-0.117)	HOMO-1 → LUMO+1; HOMO-2 → LUMO+1
S_9	4.8852	253.79	0.1275	104→107 (0.654), 105→107 (0.126), 106→110 (0.133), 106→112 (-0.118)	HOMO-2 → LUMO; HOMO-1 → LUMO; HOMO → LUMO+3, +5
S_{10}	4.9466	250.64	0.0123	104→108 (0.648), 105→108 (0.131), 99→107 (0.102), 99→109 (0.145)	HOMO-2 → LUMO+1; HOMO-1 → LUMO+1; HOMO-7 → LUMO, +2

Table S10. Specific data of the top 10 excited states of **BTPP-CHO** obtained from TD-DFT calculations.

Excited state	Excitation energy (eV)	Calculate wavelength (nm)	Oscillator Strength (f)	Main orbital contributions (coefficient ≥ 0.1)	Transition Assignment (Corresponding to Orbital Number：HOMO=109，LUMO=110)
S1	2.6451	468.73	0.0232	109→110 (0.705)	HOMO → LUMO
S2	3.4459	359.80	0.0090	108→110 (0.705)	HOMO-1 → LUMO
S3	3.7430	331.25	0.0008	103→110 (0.687)	HOMO-6 → LUMO
S4	3.8103	325.39	0.9955	109→111 (0.684), 109→112 (0.163)	HOMO → LUMO+1, +2
S5	3.8536	321.74	0.1326	109→111 (-0.164), 109→112 (0.682)	HOMO → LUMO+1, +2
S6	4.0192	308.48	0.1052	106→110 (-0.479), 107→110 (0.487)	HOMO-3, HOMO-2 → LUMO
S7	4.0242	308.10	0.0883	106→110 (0.461), 107→110 (0.504)	HOMO-3, HOMO-2 → LUMO
S8	4.3079	287.81	0.0455	109→114 (0.662)	HOMO → LUMO+4
S9	4.3645	284.08	0.0602	109→113 (0.532), 109→115 (0.373)	HOMO → LUMO+3, +5
S10	4.4624	277.84	0.0089	105→110 (0.634)	HOMO-4 → LUMO

Table S11. Specific data of the top 10 excited states of **BTPP-COOEt** obtained from TD-DFT calculations.

Excited state	Excitation energy (eV)	Calculate wavelength (nm)	Oscillator Strength (f)	Main orbital contributions (coefficient ≥ 0.4)	Transition Assignment (Corresponding to Orbital Number：HOMO=121, LUMO=122)
S1	2.9870	415.08	0.0487	121→122 (0.705)	HOMO → LUMO
S2	3.8086	325.53	0.0122	120→122 (0.703)	HOMO-1 → LUMO
S3	3.8171	324.81	1.1048	121→123 (0.703)	HOMO → LUMO+1
S4	3.8805	319.50	0.0065	121→124 (0.701)	HOMO → LUMO+2
S5	4.2501	291.72	0.0741	118→122 (0.536), 121→125 (-0.441)	HOMO-3 → LUMO, HOMO → LUMO+3
S6	4.3005	288.30	0.0479	121→126 (0.672)	HOMO → LUMO+4
S7	4.3857	282.70	0.0013	119→122 (0.695)	HOMO-2 → LUMO
S8	4.3893	282.47	0.0885	121→125 (0.340), 121→127 (0.519)	HOMO → LUMO+3, +5
S9	4.5006	275.49	0.1003	121→125 (-0.340), 121→127 (0.411)	HOMO → LUMO+3, +5
S10	4.6680	265.60	0.0448	120→124 (0.582)	HOMO-1 → LUMO+2

8. Break junction experiments

8.1 Blank solvent conductance test

Prior to molecular conductance measurements, a baseline test was performed using pure 1,2,4-trichlorobenzene (TCB) as the solvent, showing no characteristic conductance peaks other than the Au–Au atomic contact at 1 G_0, which confirms the absence of conductive contaminants.

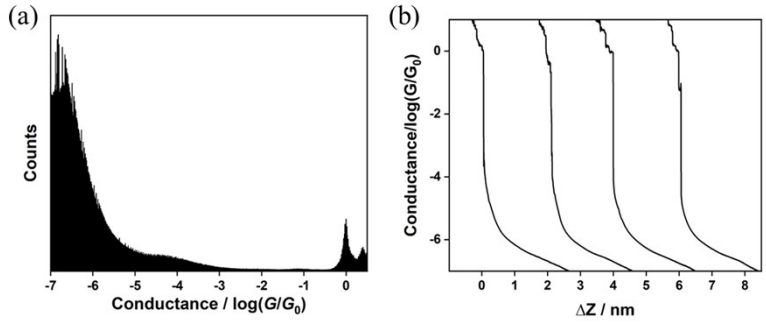

Fig. S26 (a) One-dimensional conductance histogram and molecular junction length distribution (inset) for pure TCB solvent; (b) Representative single-trace conductance-displacement curve for pure TCB.

Table S12. Conductance ($\log(G/G_0)$), *para*-Hammett constant (σ_p), Dihedral Angles θ_2, and Flicker noise analysis of **BTPP** series molecules.

Compound	Conductance ($\log(G/G_0)$)	Standard deviation	*para*-Hammett constant (σ_p)	Dihedral angles θ_2 (°)	Flicker noise analysis
BTPP-NMe$_2$	$10^{-3.39}$	0.02	−0.83	89.5	$G^{1.53}$
BTPP-OMe	$10^{-3.49}$	0.01	−0.27	59.8	$G^{1.45}$
BTPP-H	$10^{-3.52}$	0.02	0	58.6	$G^{1.77}$
BTPP-F	$10^{-3.54}$	0.03	0.06	58.4	$G^{1.50}$
BTPP-CHO	$10^{-3.69}$	0.02	0.42	54.9	$G^{1.74}$
BTPP-COOEt	$10^{-3.81}$	0.01	0.45	56.0	$G^{1.68}$

8.2 Flicker Noise Analysis of BTPP Series Molecular Junctions

In this paper, a systematic analysis of flicker noise in **BTPP** series molecules is carried out to reveal the molecule-electrode coupling mechanism.

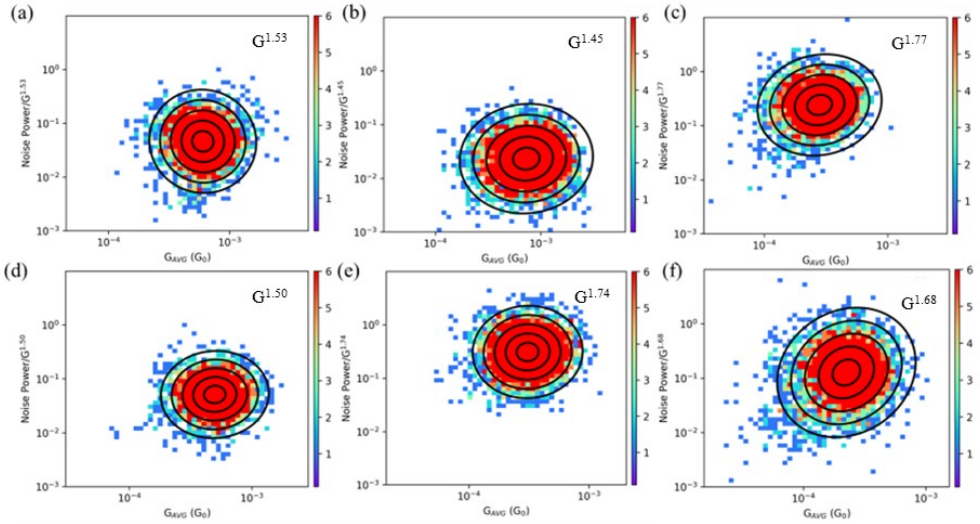

Fig. S27 Flicker noise analysis of (a) **BTPP-NMe$_2$** (b) **BTPP-OMe** (c) **BTPP-H** (d) **BTPP-F** (e) **BTPP-CHO** and (f) **BTPP-COOEt**.

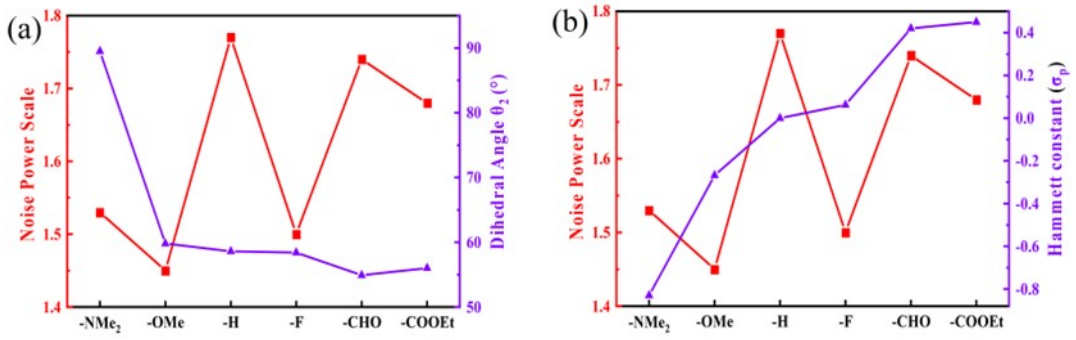

Fig. S28 Noise power scale (left y-axis) and corresponding structural/electronic properties (right y-axis) of **BTPP**-series molecules with different substituents: (a) Correlation with dihedral angle θ_2 and (b) Correlation with *para*-Hammett constant σ_p.

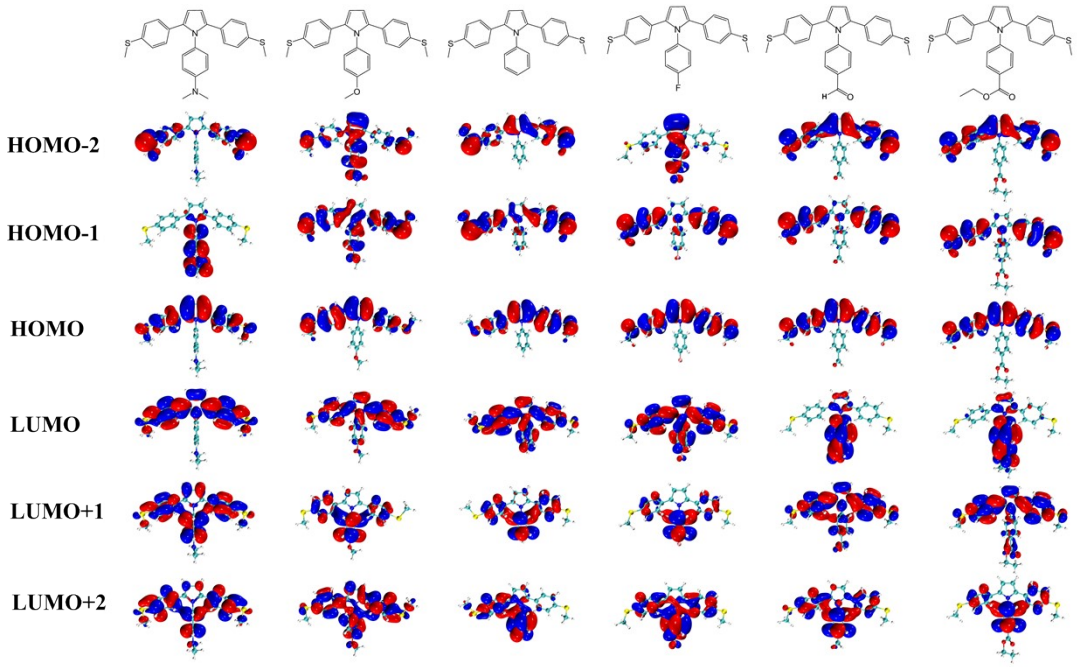

Fig. S29 Spatial distributions of frontier molecular orbitals. The isosurface value is set to 0.02.

8.3 Structural Relaxation Diagrams of BTPP derivatives

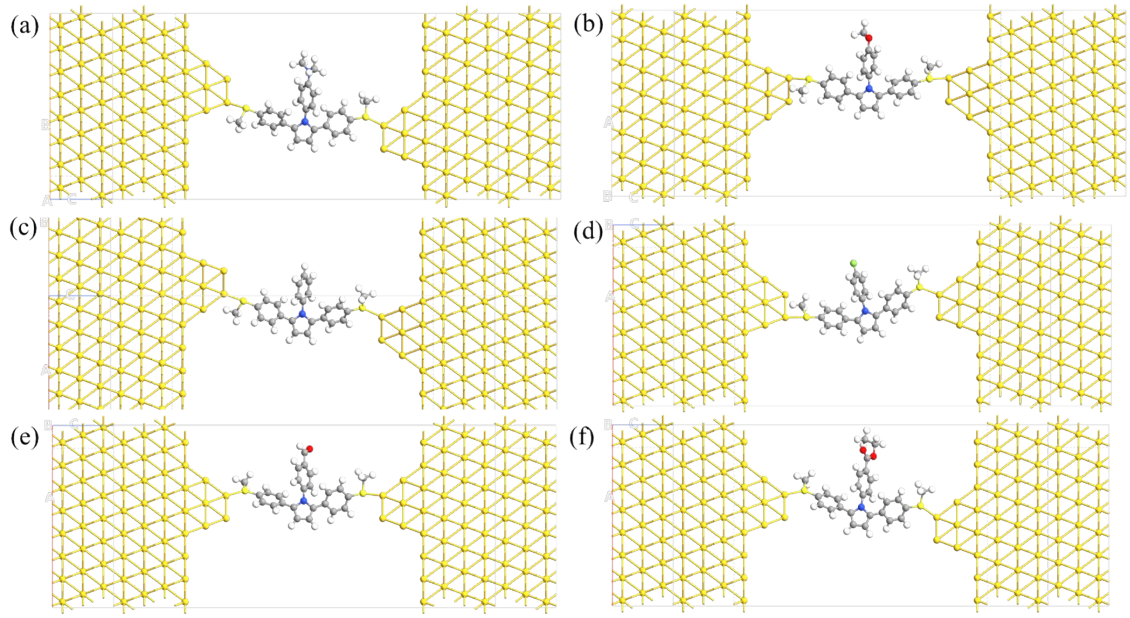

Fig. S30 Optimized molecular structures of (a) **BTPP-NMe$_2$** (b) **BTPP-OMe** (c) **BTPP-H** (d) **BTPP-F** (e) **BTPP-CHO** and (f) **BTPP-COOEt**.

References

1. H. J. Deng, Y. J. Fang, G. W. Chen, M. C. Liu, H. Y. Wu and J. X. Chen, *Appl. Organomet. Chem.*, 2012, **26**, 164-167.
2. T. Okumi, A. Mori and K. Okano, *Chem. Commun.*, 2023, **59**, 1046-1049.